Applied Catalysis A: General 532 (2017) 1–11

Contents lists available at ScienceDirect

Applied Catalysis A: General

journal homepage: www.elsevier.com/locate/apcata

Feature Article

Thermal treatments of precursors of molybdenum and vanadium oxides and the formed $Mo_xV_yO_z$ phases active in the oxydehydration of glycerol

Luiz G. Possato [a], Wellington H. Cassinelli [a], Camilo I. Meyer [b], Teresita Garetto [b], Sandra H. Pulcinelli [a], Celso V. Santilli [a], Leandro Martins [a,*]

[a] Instituto de Química, UNESP – Univ. Estadual Paulista, Rua Prof. Francisco Degni 55, 14800-060 Araraquara, SP, Brazil
[b] GICIC (Grupo de Innvestigacioes en Ciencia e Ingenieria Cataliticas) INCAPE-UNL-CONICET, Colectora Ruta Nac, 168, Santa Fe, Argentina

ARTICLE INFO

Article history:
Received 1 September 2016
Received in revised form 4 December 2016
Accepted 9 December 2016
Available online 11 December 2016

Keywords:
Glycerol oxydehydration
Acrolein
Acrylic acid
Vanadium oxide
Molybdenum oxide

ABSTRACT

This paper presents an *in situ* study of the crystallographic phases formed during the thermal treatment of precursors of vanadium and molybdenum oxides, measured under synchrotron X-ray diffraction. The interest in the speciation of $Mo_xV_yO_z$ mixed oxides lies in the excellent catalytic performance of these materials for the selective conversion of glycerol to acrylic acid employing the oxydehydration reaction. The crystallographic structure of the active phases of $Mo_xV_yO_z$ directly influences on the nearby metal valence and, therefore, on the dynamic changes in metal oxidation states during the catalytic reaction. In the present study, the thermal treatment of a mixture of the precursors of Mo and V under oxidizing or inert atmospheres revealed the major formation of 61% of MoV_2O_8 or 29% of $Mo_4V_6O_{25}$, respectively, at a final temperature of 500 °C. The most active phase for acrylic acid formation was MoV_2O_8 (3.5 times more active than the separate metal oxides), due to the instability of the phase with respect to framework oxygen at the reaction temperature. The cycle of reduction and oxidation of the vanadium in MoV_2O_8 during the reaction caused pronounced dynamic formation of oxygen vacancies, resulting in 97% conversion of glycerol and 32% selectivity towards acrylic acid.

1. Introduction

Acrylic acid is a valuable compound that is currently produced in two separate reactors by gas-phase oxidation of propylene to acrolein, and then oxidation of acrolein to acrylic acid. The total annual global production of the compound is more than 3 million tons [1]. However, in recent years, the increase in biodiesel production has resulted in vast quantities of co-produced glycerol, and many studies have been conducted aiming to produce more chemically versatile compounds from glycerol, including acrylic acid [1].

The formation of acrylic acid from glycerol occurs in two catalytic steps. In the first step, glycerol is dehydrated to acrolein on acid sites [2–13]. The second step is the selective oxidation of acrolein to acrylic acid, catalyzed by redox sites [14–24]. The combination of these two reaction steps using a single bifunctional catalytic bed (the oxydehydration reaction) offers advantages including the ideal thermal balance provided by coupling the exothermic oxidation reaction with the endothermic dehydration reaction [2,25,26].

Vanadium and molybdenum oxides provide both active sites (redox and acid) and exhibit intermediate catalytic properties for a number of selective oxidation reactions. The acid sites are due to the vanadium or molybdenum cations, and the oxidation reaction performed by the redox sites takes place via a three-step process, known as the Mars – van Krevelen mechanism [27] as follows:

(1) First, the adsorbed organic reactant is oxidized by a mobile oxygen ion present in the lattice of the catalyst ($M^{(n+1)+}O_x \rightarrow M^{n+}O_{x-1}$), followed by desorption of the product (in the present case is acrylic acid);
(2) In a second step, the oxygen vacancy migrates from its origin by relocation of the surrounding lattice oxygen atoms;
(3) Finally, a dioxygen molecule from the gas phase restores the fully oxidized state of the catalyst ($M^{n+}O_{x-1} \rightarrow M^{(n+1)+}O_x$).

However, in order to be efficiently used in glycerol oxydehydration, the redox properties of the pure vanadium or molybdenum

* Corresponding author.
E-mail address: leandro@iq.unesp.br (L. Martins).

http://dx.doi.org/10.1016/j.apcata.2016.12.010
0926-860X/

oxides need to be improved. For example, the use of vanadium oxide as catalyst in glycerol oxydehydration at 300 °C gave 5% of acrylic acid for 40% glycerol conversion. Molybdenum oxide provided comparable performance. However, under the same reaction conditions, the use of V/Mo mixed oxides gave 20% of acrylic acid for nearly complete conversion of glycerol [28]. Enhanced selectivity towards acrylic acid, of 28% and 50%, was achieved using V/Mo/Te/Nb oxides and V/W/Nb oxides, respectively [29–31]. The explanation for the superior performance of the latter two catalysts is that both the redox cycle and the strength of the acid sites are improved. These examples illustrate some of the reasons for research concerning the synthesis of active $Mo_xV_yO_z$ oxides that could act as efficient multifunctional catalysts for glycerol oxydehydration.

There are three important complementary aspects involved in the synthesis of catalysts for glycerol oxydehydration, which are the structure of the active phase (and therefore the coordination geometry), the nearby metal valence, and the dynamic changes in oxidation states of the metal during catalytic reaction via the Mars – van Krevelen mechanism. Shen et al. [28] prepared V/Mo and V/W catalysts by calcination of mixtures of salts, and the presence of vanadium was found to promote the formation of greater quantities of partially reduced species, such as Mo^{5+}, W^{5+}, and V^{4+}, compared to the pure oxides MoO_3, WO_3, and V_2O_5. Formation of the crystalline $Mo_6V_9O_{40}$ phase was shown to be positive for acrolein oxidation to acrylic acid, the higher the content of vanadium in the catalysts the higher the selectivity towards oxygenated products [32,33].

All these interesting aspects highlight the necessity to understand the controlling steps in the preparation of catalysts for glycerol oxydehydration. In this study, we describe glycerol oxydehydration catalyzed by vanadium and molybdenum mixed oxides prepared by thermal treatment using different temperatures and atmospheres (N_2 or O_2 in N_2). The development of the crystalline $Mo_xV_yO_z$ active phase and the formation of V^{5+}/V^{4+} or Mo^{6+}/V^{4+} oxidation states were monitored by *in situ* X-ray powder diffraction (XRD), X-ray absorption spectroscopy (XAS) in the XANES region, and X-ray photoelectron spectroscopy (XPS).

2. Experimental

2.1. Preparation of the catalysts

The mixed molybdenum-vanadium oxides were obtained using a mixed aqueous solution of ammonium metavanadate (NH_4VO_3, Sigma Aldrich, 99%) and ammonium paramolybdate ($(NH_4)_6Mo_7O_{24}$, Synth, 83%). A 200 mL solution containing up to 2 g of the salts, added in different proportions, was stirred and dried at 40 °C in a rotary evaporator, then calcined at 500 °C for 2 h (using a heating rate of 5 °C/min) under N_2 or an O_2/N_2 mixture (20/80%). The Mo/(V + Mo) compositional fractions employed were 0 (sample A, pure vanadium oxide), 0.2 (sample B), 0.4 (sample C), 0.6 (sample D), 0.8 (sample E), and 1 (sample F, pure molybdenum oxide). The bare oxides were prepared by calcination of the NH_4VO_3 and $(NH_4)_6Mo_7O_{24}$ salts. The heating atmosphere depended on the use: for the catalytic tests – (a) 80% N_2 and 20% O_2 or (b) 100% N_2, while for *in situ* XRD experiments – (a) 80% He and 20% O_2 or (b) 100% He.

2.2. Characterization of the catalysts

In situ X-ray powder diffraction (XRD) analysis was carried out during heating of the V-Mo salts under flows of He or 20% of O_2 in He at the XPD beamline of the Brazilian Synchrotron Light laboratory (LNLS). XPD beamline had a Huber 4 + 2 circle diffractometer equipped with an Eulerian cradle (model 513) placed *circa* of 13 m from the double-bounce Si(111) monochromator (λ = 1.377 Å) [34]. The data were collected in the high-resolution mode employing a Si(111) analyzer crystal and a Mythen detector. Thermal treatment was performed from room temperature up to 500 °C, at a heating rate of 5 °C/min, using a furnace to which a mass spectrometer was coupled in order to monitor the outflowing products. The measurement of each diffraction pattern occurred in the 2θ interval between 20° and 30°, and it took 2 min. A wide range scan from 7 to 60° should be used for a more precise phase analysis. However, under the heating ramp of 5 °C/min, it would be impossible to have a temporal resolution and to follow the transitions between many crystallographic phases. Previous scans of a few regions indicated that the 2θ range from 20 to 30° was the most appropriate to have a good compromise between quality of the refinement and the number of acquired scans. In fact, refinement of full diffractograms of samples treated at every 100 °C (Fig. S1) showed very similar results. Although thermal activation of the precursors was performed under 60 mL/h flow of N_2 or 20% of O_2 in N_2 during the catalytic oxydehydration experiments, the use of helium was required in the *in situ* XRD studies in order to enable mass spectrometric determination of the products (such as NH_3 and/or N_2) released from decomposition of the precursors.

Conventional X-ray powder diffraction (XRD) patterns of the calcined mixed oxides were acquired using a Siemens D5000 diffractometer, with Cu-Kα radiation selected by a curved graphite monochromator. Data were collected in the 2θ range from 5° to 60°, with a scan step of 0.01° and counting time of 4 s. Quantitative phase analysis was performed by the Rietveld profile method, using GSAS-EXPGUI software [35,36]. The scale factors, zero shifts, and backgrounds of the peak profiles and the lattice parameters were refined using a sixth-degree Chebyshev polynomial. Pseudo-Voigt functions were employed for the peak profile refinements. Other parameters were not refined.

The thermal behavior of samples was investigated by thermogravimetric analysis (TGA), performed from room temperature up to 650 °C under N_2 or 20% of O_2 in N_2 flow (50 mL/min), by using a SDT600 TA Instruments at a heating rate of 10 °C/min.

Nitrogen gas adsorption-desorption isotherms were measured at liquid nitrogen temperature (−196 °C) and relative pressure interval between 0.001 and 0.998, using a Micromeritics ASAP 2010 system. The samples were pretreated under vacuum ($\sim 10 \times 10^{-6}$ Pa) at 200 °C for 12 h. Surface areas (S_{BET}) were determined by the BET method [37].

Temperature-programmed desorption of ammonia (NH_3-TPD) was used to quantify the acid sites present on the oxide catalysts. The samples (150 mg) were first kept in a flow of helium (60 mL/min) at 300 °C for 1 h, and then cooled to 100 °C. In the next step, adsorption of NH_3 was achieved by exposing the samples to a flowing gas mixture of 1% NH_3/He (60 mL/min) for 1 h, until saturation was reached. This was followed by flushing with helium at 100 °C for 1 h to remove the excess of NH_3. Temperature-programmed desorption was performed from 100 °C up to 550 °C, using a heating ramp of 10 °C/min and a 60 mL/min flow of helium. Quantification of the ammonia desorbed during heating was achieved using the signal from a mass spectrometer (Balzers Omnistar).

XPS measurements of the Mo-V oxides were performed using a UNI-SPECS UHV spectrometer with Mg-Kα source (λ = 1253.6 eV), pass energy of 10 eV, and 0.2 eV energy step. The pelleted samples were first left overnight under vacuum (<3.7×10^{-11} Pa), after which the analysis was performed at a residual pressure below 3.7×10^{-11} Pa inside the chamber. The binding energies of the chemical elements were determined by fitting the measured spectra and referencing to the C 1 s (285.1 eV) peak, with accuracy of ±0.1 eV. The fitting of the curves was performed with CasaXPS soft-

ware, using the Shirley baseline function and Voigt profile (70% Gaussian and 30% Lorentzian).

X-ray absorption spectroscopy (XAS) measurements were recorded at the V and Mo K-edge in transmission mode at the XAFS1 beamline of the Brazilian Synchrotron Light laboratory (LNLS). The XAFS1 beamline is equipped with two monochromators (Si (111) and Si (220) for vanadium and molybdenum analyses, respectively), operated in Bragg mode, for selection of the desired range of X-ray wavelengths. The monochromators were calibrated by setting the first inflection point at the K-edge spectrum of the corresponding metallic foil standard (5465 eV for vanadium and 20000 eV for molybdenum). The powdered samples, diluted with boron nitride (BN), were presented in the form of pellets (20 mg) whose thickness was chosen so that the absorption jump at the edge was close to 1.

Analysis of the XAS data using the Athena graphical interface software enabled speciation of the vanadium and molybdenum by means of linear combinations (LC) of the spectra (from −20 to 120 eV around the edge), using three merged spectra in order to improve the signal-to-noise ratio. The references used for treating the spectra were V_2O_4, V_2O_5, MoO_3, MoO_2, and vanadium and molybdenum metallic foils.

The ^{13}C nuclear magnetic resonance (MAS NMR) analysis was performed using a Bruker Avance III 400 MHz WB instrument, equipped with a 4 mm probe and operated with a rotor speed of 15 kHz. The spent catalysts (after the reaction) were placed into a 4 mm zirconia rotors, using the same volume of sample. The experimental conditions were a contact time of 2000 s, a pulse width of 2.4 s, and a frequency of 12 kHz.

The Infrared spectroscopy (FTIR) was done using a Shimadzu Prestige IR apparatus. More detailed experimental procedure was published elsewhere [3,4].

2.3. Glycerol oxydehydration

The glycerol oxydehydration reaction, carried out at 300 or 350 °C and atmospheric pressure, used 200 mg of a finely divided powder of the catalyst deposited on a fixed bed inside the glass reactor. No diluent was used. The reaction temperature was monitored with the aid of a thermocouple in contact with the catalytic bed. The sample was firstly heated to the reaction temperature under a mixed flow of nitrogen and oxygen (at 24 and 6 mL/min, respectively) and kept at this temperature for 15 min. The samples calcined in N_2 were heated under N_2 flow (30 mL/min) before the tests. A solution of 10 wt.% glycerol (Sigma-Aldrich, 99%) in water was continuously introduced (at 0.05 mL/min) to the gas line using a syringe pump (KD Scientific). The space velocity was of 5 h^{-1}. The effluent products, collected in a gas-liquid separator kept at 1 °C, were analyzed using a gas chromatograph (Shimadzu GC-2014) equipped with a capillary column (Rtx-1, 30 m, 0.32 mm, 1 μm) and FID detector. A very low temperature in the gas-liquid separator aimed to ensure the condensation of the more volatile compound (acetaldehyde, b.p. of 20 °C). Moreover, before each injection, a known mass of n-butanol was added as internal standard to guarantee a quantitative mass balance for condensed products. The analyses were carried out in triplicate and the retention times were compared to those of authentic compounds. Conversion of glycerol ($X_{glycerol}$) and products selectivity (S) were calculated according to Eqs. (1) and (2):

$$X_{glycerol}(\%) = \frac{{n_{Gl}}^{input} - {n_{Gl}}^{output}}{{n_{Gl}}^{input}} \times 100 \quad (1)$$

$$S_i(\%) = \frac{n_i}{{n_{Gl}}^{input} - {n_{Gl}}^{output}} \times \frac{Zi}{Z_{Gl}} \times 100 \quad (2)$$

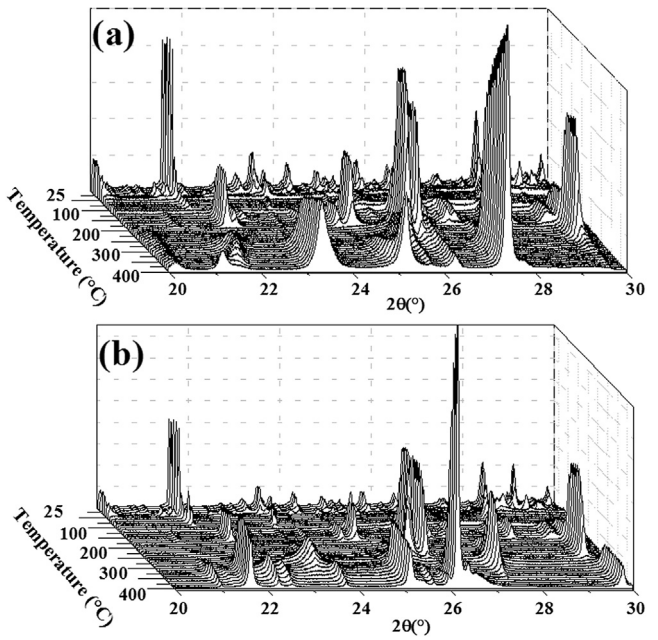

Fig. 1. *In situ* XRD patterns of sample D (molybdenum mole fraction = 0.6) obtained using (a) oxidizing (20% of O_2 in He) and (b) inert atmospheres (100% of He).

where ${n_{Gl}}^{input}$ and ${n_{Gl}}^{output}$ are the molar flows of glycerol (mol/min) in the input and output, respectively; n_i is the molar flow of product *i* (mol/min); $Z_{Gl} = 3$ is the number of carbon atoms in the glycerol molecule; and Z_i is the number of carbon atoms in the product *i*. Finally, the selectivity to CO and CO_2 was calculated by a carbon balance considering the mole flow of glycerol fed to the reactor and the mole flow of non-converted glycerol and products leaving the reactor, which was likely because no residual carbon deposit (coke) was detected in the spent catalysts.

The estimation of the V_2O_5 and MoO_3 specific activity was done separately by considering the pure oxides. For the sample of mixed oxides the contribution of MoV_2O_8 was calculated by taking into account the relative proportion of V_2O_5, MoO_3 and MoV_2O_8 obtained from the refinement analysis.

3. Results and discussion

3.1. Thermal decomposition of precursors of vanadium and molybdenum oxides monitored by TGA and by in situ XRD

The preparation of the molybdenum and vanadium mixed oxides involved the thermal decomposition of a mixture of NH_4VO_3 and $(NH_4)_6Mo_7O_{24}$ salts, heated from room temperature to 500 °C. The crystalline phases detectable in the representative 2θ region between 20 and 30°, formed during thermal treatment of sample D (Mo mole fraction = 0.6) under oxidizing (O_2/He) and inert (He) atmospheres, are displayed in Fig. 1a and b, respectively. Sample D was chosen for an in depth analysis, because it was the most active sample in glycerol oxydehydration. Quantitative temporal analysis of the different crystalline phases was performed after applying the Rietveld refinement method, as shown in Fig. 2, with the outflowing gases monitored by a mass spectrometer coupled to the exit of the furnace. Table 1 lists the crystalline compounds and the JCPDS PDF (powder diffraction files) associated with the thermal decomposition of the mixed precursors of molybdenum and vanadium as a function of temperature and atmosphere. The thermogravimetric curves (TGA) obtained for sample D in different atmospheres (Fig. 3) provide complementary data for the results shown in Figs. 1 and 2.

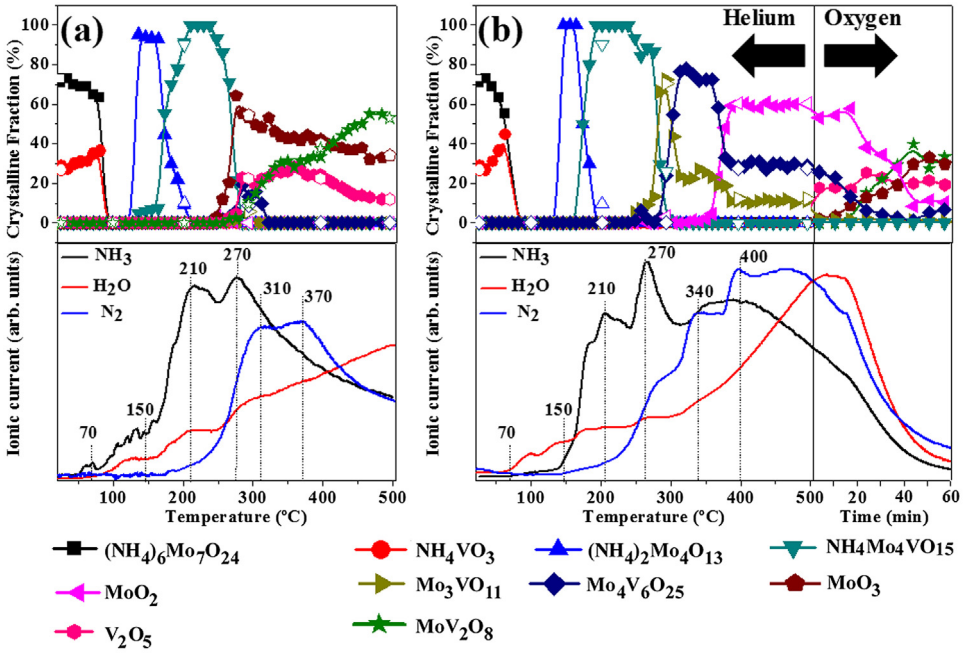

Fig. 2. Speciation of the crystallographic phases and outflowing gases detected by mass spectroscopy during the thermal activation of sample D in (a) oxidizing (20% of O_2 in He) and (b) inert atmospheres (100% of He). The empty points represent the quantitative phase analysis of full diffractograms in the 2θ region from 7 to 60° of samples treated at every 100 °C.

Table 1
Crystalline compounds involved in the cooperative thermal decomposition of mixed vanadium and molybdenum salts (sample D, molybdenum mole fraction = 0.6). See Figs. 1 and 2.

Crystalline compounds	JCPDS PDF	Temperature (°C)	Atmosphere	Stoichiometric oxidation state	
				Vanadium	Molybdenum
Precursors					
$(NH_4)_6Mo_7O_{24}$	70–0957	RT	He and O_2/He	...	6
NH_4VO_3	01–0762	RT	He and O_2/He	5	...
Decomposition products					
Amorphous species	...	100	He and O_2/He	5	6
$(NH_4)_2Mo_4O_{13}$	80–0757	150	He and O_2/He	...	6
$NH_4Mo_4VO_{15}$	73–0039	200	He and O_2/He	5	6
MoV_2O_8 (main compound)	20–1377	300	O_2/He	5	6
MoO_3	65–2421	300	O_2/He	...	6
V_2O_5	41–1426	300	O_2/He	5	...
Mo_3VO_{11}	13–0142	300	He	4	6
$Mo_4V_6O_{25}$ (main compound)	19–0812	300	He	4.3	6
MoO_2	05–0452	400	He	...	4

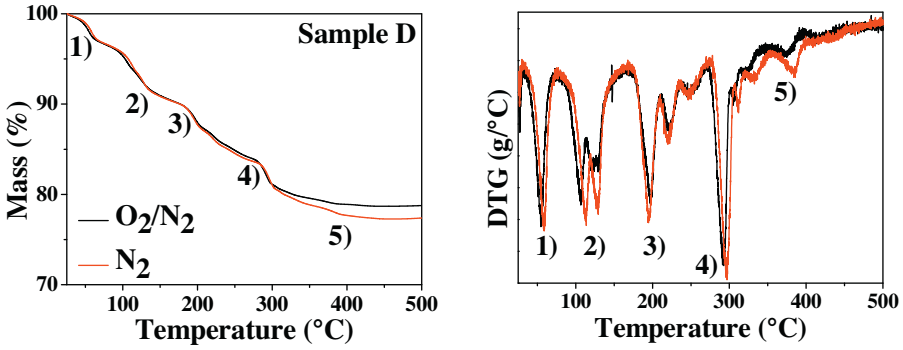

Fig. 3. Thermogravimetric and differential thermogravimetric analysis curves obtained for sample D in oxidizing (20% of O_2 in N_2) and inert atmospheres (100% of N_2). The indicated temperatures relate to events occurring at 1) 70, 2) 150, 3) 210, 4) 270, and 5) >300 °C.

The quality of the refined diffractograms measured in the 2θ region from 20 to 30° (close symbols in Fig. 2) was compared with those obtained from diffractograms measured in the full 2θ region from 7 to 60° (open symbols in Fig. 2); the results were very similar. A

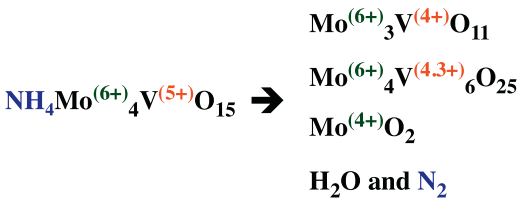

Scheme 1. Possible intermediates during the transformation of $NH_4Mo^{(6+)}{}_4V^{(5+)}O_{15}$ in temperatures above 270 °C.

sketch of the intermediary and final crystalline phases is presented in Fig. S2 (supplementary material).

Initial evaluation of the X-ray diffractograms gave a strong indication that thermal decomposition in the different environments resulted in differences in the vanadium and molybdenum catalysts at the end of the process. Analysis of the combined results revealed five key events, centered at 70, 150, 210, 270, and >300 °C. Below 270 °C, both atmosphere conditions resulted in similar behavior in terms of the crystallographic fingerprints as well as the mass spectrometry profiles and TGA curves.

The first transformation event, detectable by both TG analysis (Fig. 3) and the corresponding *in situ* XRD speciation (Fig. 2), indicated that the precursors were converted to amorphous intermediate phases at the same time that water was released. This was supported by the complete disappearance of the XRD peaks. The explanation for the complete amorphization at 100 °C relies on the melting points of a eutectic solution of salts possessing the same NH_4^+ cations, $(NH_4)_6Mo_7O_{24}$ (melts at 90 °C) and NH_4VO_3 (at 200 °C).

In the second thermal transformation step, structural NH_4^+ cations were decomposed to ammonia, generating the crystallographic phase of a solid corresponding to $(NH_4)_2Mo_4O_{13}$. The decrease of the NH_4^+/Mo^{6+} molar ratio from 0.85 (for the precursor) to 0.50 is indicative of the release of ammonia. Although not detected by XRD, a similar decomposition was likely for NH_4VO_3, because the weight loss for the temperature range used exceeded the loss expected considering only the change in molybdenum salt stoichiometry from 6% to 9% (in step 2 shown in Fig. 3).

In the third step, at around 210 °C, the $NH_4Mo_4VO_{15}$ crystallographic phase was formed and the NH_4^+/metal molar ratio decreased again to 0.2. In the fourth decomposition step, at about 270 °C, the first differences appeared between the decomposition profiles obtained under the two atmospheres. From this point onwards, the mixed oxides acquired crystallographic patterns and oxidation states appropriate to the gas environments, with the $NH_4Mo_4VO_{15}$ phase seeming to be a key compound on which the formation of the subsequent phases depended.

In the temperature range between 270 °C and 500 °C, the release of NH_3 caused changes in the oxidation states of vanadium and molybdenum, the atmosphere used having a determining influence on this process. The progressive temperature increase caused an increase of N_2 production at 270 °C, due to reduction of V^{5+} to V^{4+} and Mo^{6+} to Mo^{4+}, promoted by NH_3 (Scheme 1). A greater quantity of water was released in the presence of helium, and the residual mass after the TGA was considerably smaller. Comparison of the elements showed that vanadium was more easily reducible ($Mo^{(6+)}{}_3V^{(4+)}O_{11}$ is formed at 300 °C) than molybdenum ($Mo^{(4+)}O_2$ is only formed at 350 °C), in agreement with the lower reduction potential of vanadium, compared to molybdenum.

For the oxidizing atmosphere and above 300 °C, the concurrence between the oxidation and reduction reactions promoted by the outflowing gases led to a decreased overall profile of N_2. Stoichiometric analysis of the compounds listed in Table 1 showed that under O_2/He, vanadium and molybdenum remained oxidized as +5 and +6, respectively. A comparative analysis of the X-ray absorption spectra for vanadium and molybdenum at the end of the oxidation at 500 °C (Fig. 4) confirmed the metal valences, with the spectra being very similar to those of V_2O_5 and MoO_3. In the case of the vanadium edge, the three samples (two standards and sample D) showed small pre-edge 1s to 3d ground-state transitions. However, in contrast, comparison of the V_2O_4 spectrum with that of sample D revealed no significant congruency in the oscillatory scatterings in the XANES region (above approximately 5490 eV). For molybdenum, the spectrum of sample D was indicative of the presence of MoO_3, because the pre-edge is absent in the case of MoO_2 [38].

It could be concluded from these results that under an O_2/He atmosphere, the predominant mixed oxide at the end of the thermal treatment was the orthorhombic MoV_2O_8 (around 61%), together with V_2O_5 and MoO_3. However, under He, the main mixed oxide was $Mo_4V_6O_{25}$ (29%), together with Mo_3VO_{11} (11%) and MoO_2 (60 %). In an attempt to obtain MoV_2O_8, the gas flow was changed from He to O_2/He at 500 °C. There was a progressive change in speciation (Fig. 2), with MoV_2O_8 stabilizing at 33%, which was half the amount obtained previously under a constant O_2/He atmosphere [39–42].

3.2. Speciation of the crystallographic phases of mixed oxides prepared with different proportions of vanadium and molybdenum precursors

The XRD patterns and the quantitative phase analysis results obtained from the Rietveld refinement of samples with different proportions of precursors are shown in Fig. 5 and 6. The precursors were thermally treated under 20% of O_2 in N_2 atmosphere. The V_2O_5 oxide showed the most intense diffraction peaks related to (200), (001), (101) and (110) crystallographic reflections. The MoO_3 sample showed diffraction peaks associated to (200), (101), (400) and (210). Both phases have orthorhombic structures, facilitating the isostructural exchange of elements. Furthermore, despite the larger atomic radius of molybdenum than vanadium, the lower valence of vanadium (V^{4+}) makes the metal-oxygen bond distances closely similar for both elements in the MoV_2O_8 structure [43]. For the Mo-V samples, the most intense peaks (hkl) of V_2O_5 disappeared and new diffraction peaks were present. This suggests that a mixed oxide structure was obtained, and that the new peaks at 18.2, 21.5, and 25.0° are due to the orthorhombic MoV_2O_8 structure. Other possible structures were tentatively explored, such as $MoVO_5$ (PDF 18-0852), $(Mo_{0.7}V_{0.3})_2O_5$ (PDF 21-0576), and $(MoV)_5O_{14}$ (PDF 01-0074), but no associated diffraction hkl planes were present.

The phase quantification of the Mo-V samples, performed using the Rietveld refinement method, resulted in the mass composition of the crystalline fraction as a function of the molybdenum molar fraction (Fig. 6). Despite the fact that the MoV_2O_8 structure is rich in vanadium (2 V:1Mo), more of it was formed for samples that originally contained more molybdenum. A possible explanation for the best Mo/(V + Mo) mole ratio of 0.6 is that the formation of the transitional $NH_4Mo_4VO_{15}$ structure, which precedes the MoV_2O_8 structure, was kinetically limited by the quantity of molybdenum species of 4:1.

As mentioned above, in the MoV_2O_8 oxide, molybdenum and vanadium are present in their maximum oxidation states (+6 and +5, respectively). Nonetheless, structural defects can occur, because in octahedral coordination the V^{5+} ionic radius (6.2 pm) is somewhat smaller than that of the molybdenum cation (6.8 pm) [44]. As a result, some of the vanadium atoms can be reduced to V^{4+}, which improves the atomic arrangement, and then remain with reduced valence of +4. These results are in agreement with the recent findings of Shen *et al.* [28], who observed that some of the vanadium atoms are present as V^{4+} in Mo/V and W/V mixed oxides, which supports the formation of mixed oxides with lower valence of vanadium. In fact, changes in the oxidation states of the metallic elements comprising the mixed oxides are a critical feature of

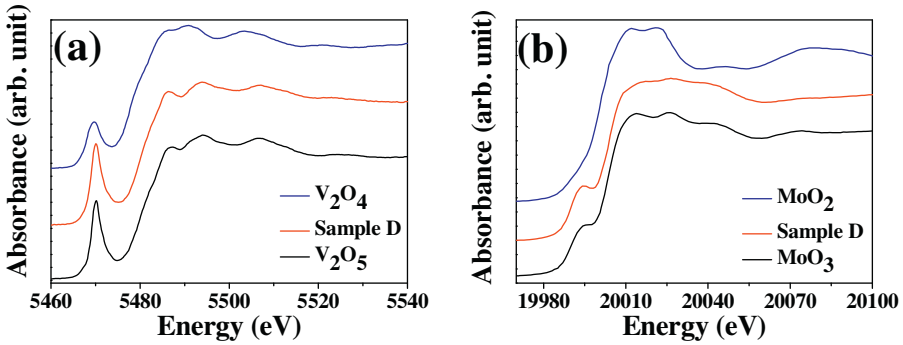

Fig. 4. Comparison of X-ray absorption spectra in the K-edge region for the thermally treated sample D and oxide standards of known valence: (a) vanadium; (b) molybdenum.

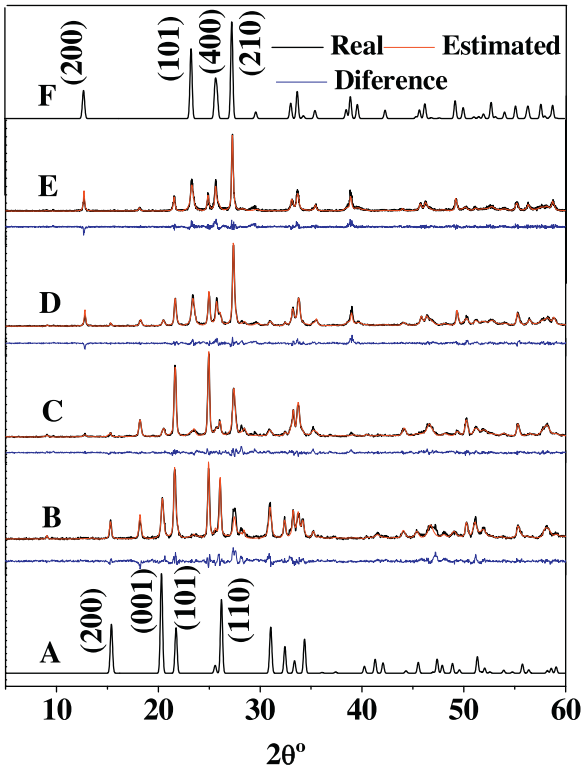

Fig. 5. X-ray powder diffractograms of V_2O_5 (A), MoO_3 (F), and the mixed oxides of vanadium and molybdenum. The net results of the Rietveld analyses are shown in red, and the deviations from the measured diffractograms are in blue. (For interpretation of the references to colour in this figure legend, the reader is referred to the web version of this article.)

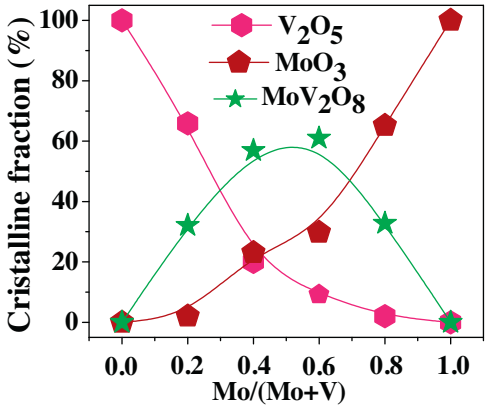

Fig. 6. Results of quantitative phase analysis obtained from Rietveld refinement for precursors thermally treated under 20% of O_2 in N_2 atmosphere.

Table 2
Oxidation states of vanadium and molybdenum mixed oxides, treated at 500 °C under an O_2/He atmosphere, determined by X-ray photoelectron spectroscopy (XPS) and X-ray absorption spectroscopy (XAS).

Catalyst	Mo fraction (XPS)	XPS V^{4+} (%)	XAS V^{4+} (%)	XPS and XAS Mo^{6+}
A (0)	0	0	0	...
B (0.2)	0.41	23	1.4	100
C (0.4)	0.57	25	7.9	100
D (0.6)	0.74	27	8.4	100
E (0.8)	0.82	30	6.4	100
F (1.0)	1.00	...	...	100
D-spent[a]	0.73	40	...	100

[a] Results for spent catalyst D after the oxydehydration of glycerol at 300 °C.

glycerol oxidation according to the Mars – van Krevelen mechanism [27].

The results of the XAS and XPS analyses provided information concerning the oxidation states of vanadium and molybdenum in samples A-F treated at 500 °C (Table 2). The XAS spectra were submitted to linear combination fittings, using spectra for relevant reference compounds (V_2O_5, V_2O_4, MoO_3, and MoO_2). The chemical speciation showed that the valence of molybdenum remained invariant, while the proportion of V^{4+} varied systematically, with a maximum of 8.4% for sample D. When the quantity of MoV_2O_8 increased the vanadium +4 valence also increased. According to the stoichiometry of MoV_2O_8, vanadium bears the valence +5. However, the accommodation of vanadium atoms in the structure MoV_2O_8 allows its reduction to V^{4+}. Thus, the higher amounts of the MoV_2O_8 phase in samples D and E are associated with increased V^{4+} in these catalysts. The formation of vanadium in a lower oxidation state is associated with the nature of the chemical environment in which the MoV_2O_8 mixed oxide phase is produced [43,45].

The XPS results indicated the same general trends for V^{4+}. Due to the limited sampling depth that is an inherent feature of the technique, it was clear that the anionic vacancies (and, consequently, the nonstoichiometric MoV_2O_{8-z} microdomains) were located adjacent to the surface of the solid. It could be concluded from the combined results of the characterization techniques that the partial removal of oxygen anions from MoV_2O_8 did not change the crystallographic pattern. Consequently, the MoV_2O_8 structure seems to be sufficiently flexible to accommodate the anionic vacancies without structural collapse, with fast oxygen transfer and oxygen/vacancy diffusion through the active surface [45,46]. Although the XPS results concerning the vanadium core could be affected by X-ray beam exposure due to ionization effects, the quantification of V^{4+} described herein is very similar to that of the reference 27. In fact, the XPS results helped us to support that the structure of the crystalline mixed oxide influences in the vanadium oxidation state [47,48].

Table 3
Surface area (S_{BET}) and ammonia desorption results for bare and mixed Mo-V oxides treated under 20% O_2/N_2 or 100% N_2.

Catalyst	Calcined in 20% of O_2 in N_2		
	S_{BET} (m^2/g)	μmol NH_3/g	μmol NH_3/m^2
A (0)	7.6 ± 0.2	67	9
B (0.2)	9.3 ± 0.1	574	62
C (0.4)	6.7 ± 0.2	542	81
D (0.6)	0.4 ± 0.1	510	1275
E (0.8)	0.4 ± 0.1	492	1230
F (1.0)	0.5 ± 0.1	427	854
D-N_2 (0.6)[a]	0.5 ± 0.1	39	79

[a] The sample treated under 100% N_2 flow forms preferentially the phase $Mo_4V_6O_{25}$.

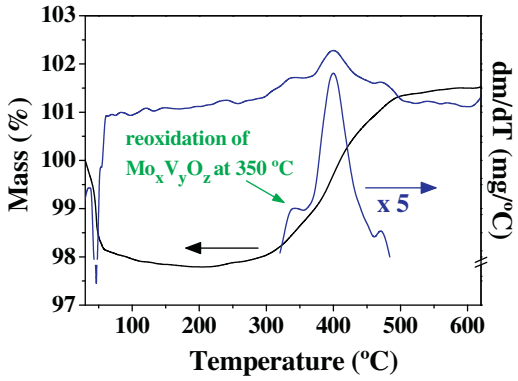

Fig. 7. Thermogravimetric analysis of spent sample D under oxidizing flow (20% of O_2 in N_2).

3.3. Catalytic performance of the vanadium and molybdenum mixed oxides in the glycerol oxydehydration reaction

The formation of acrylic acid from glycerol involves two stages of reactions (Scheme 2). In the first stage, glycerol is dehydrated to 3-hydroxypropanal on acid sites, followed by subsequent dehydration and formation of acrolein. In the final stage, the oxidation of acrolein to acrylic acid occurs on metal-oxygen redox sites. For selective synthesis of acrylic acid from glycerol, the catalyst therefore requires two fundamental characteristics, namely acid and oxidant sites [49].

Prior to the catalytic experiments, the acid characteristics and surface areas of the samples of mixed oxides were characterized by desorption of ammonia (Fig. S3) as a probe molecule, and by nitrogen adsorption-desorption isotherms (using the BET equation to obtain the surface areas), respectively. The results are shown in Table 3. It is clear that the incorporation of molybdenum in the oxides lead to decrease the surface area and increase the ammonia desorption capacity, which is an indicative of correlation between these two parameters. This behavior was also perceived by Shen et al. [28] That is, despite of the decrease in the surface area, the quantity of acid sites increases. The same experiments for samples heated under N_2 showed similar surface area, however, the quantity of acid sites was much smaller, due to a reduction in MoV_2O_8 phase. Despite of the differences in acidity, the next results confirmed that the key step for the glycerol oxydehydration reaction was the oxidation of acrolein at redox sites, which are improved in the mixed oxides.

An additional effort to determine the proportion between Lewis and Brønsted acid sites consisted in the study of pyridine adsorption. The sample D calcined in O_2/N_2 atmosphere was pretreated at 350 °C for 30 min and then cooled in vacuum. The adsorption of pyridine occurred at room temperature (Fig. S4 in supplementary material). Two wide bands were detected in the IRFT spectrum at 1580 and 1490 cm^{-1}, corresponding to adsorbed pyridine in Brønsted and Lewis acid sites, respectively. As already verified by desorption of ammonia, the acid sites are very weak. In fact, the the vibration bands referred to pyridine adsorption shifted at an average of 40 cm^{-1} to higher wavenumber in comparison to catalysts possessing very strong acid sites [4]. After submitting the sample to a vacuum of 0.013 Pa, the weakly interacting pyridine is easily desorbed. Due to the very weak acid sites, the sample D calcined in N_2 atmosphere had no detectable pyridine adsorption.

Table 4 summarizes the catalytic performance under 20% of O_2 in N_2 stream of Mo-V mixed oxides treated in N_2 or O_2/N_2 atmospheres. The samples treated in O_2/N_2 provided the highest conversion of glycerol, with selectivity towards acrylic acid close to 30%. Major byproducts were acetaldehyde, acetic acid, CO, and CO_2. The selectivity towards the gases CO and CO_2 decreased with rise in the reaction temperature from 300 to 350 °C. But, the increase in reaction temperature promoted the formation of acrylic acid. These results are based on the kinetics of oxygen transfer by the vanadium-molybdenum oxides to the chemisorbed aldehyde intermediate [14]. From a thermodynamic point of view, it is expected that the rise in temperature should lead to an increase in the formation of CO and CO_2. The explanation to that discrepancy is given by the thermogravimetric measurement of the spent sample D after the glycerol oxydehydration at 300 °C (Fig. 7). The temperature of 350 °C and above is the region in which the oxygen vacancies are significantly restored. Clearly, the reoxidation of the spent catalyst at 350 °C supports that this temperature is the best temperature to keep the redox cycle of the mixed oxides and the higher selectivity to acrylic acid (and consequently lower selectivity to CO_x).

Even containing a small quantity of V_2O_5 and MoO_3, the most active phase was MoV_2O_8, due to the instability of the framework oxygen at the temperature of the reaction. The cycle of reduction and oxidation of the vanadium in MoV_2O_8 during the reaction, showing the dynamic nature of the redox mechanism and the creation of oxygen vacancies, was more important than the oxidation states of the elements after the thermal treatments. Based on the acrylic acid selectivity and the catalysis achieved by these materials, the activity of the phases increased in the order: V_2O_5 (selectivity of 10.4%), $Mo_4V_6O_{25}$ and Mo_3VO_{11} (15.8%), MoO_3 (16.0%), and finally the orthorhombic MoV_2O_8 (32.0%).

Fig. 8 displays the glycerol conversion, CO_x selectivity and selectivity towards acrylic acid after 1 h of reaction for the series of vanadium-molybdenum oxides treated in O_2/N_2 atmosphere (samples A-F). The relations between structure and performance illustrated in Figs. 6 and 8 (both showing a maximum) were also in agreement with the superior activity of the mixed oxide treated under O_2/N_2. Analysis of the results, taking into account the families of crystalline phases, gave a specific activity for bare V_2O_5 of 1.91 mg of acrylic acid/min.g of V_2O_5, while the specific activity for MoO_3 was 2.05 mg of acrylic acid/min.g of MoO_3. The performance of MoV_2O_8 was far superior, at 6.74 mg of acrylic acid/min.g of MoV_2O_8, *i.e.* 3.5 times more than for the individual oxides of the same family.

The sample calcined in pure nitrogen atmosphere (sample D-N_2) did not show the same catalytic activity. Even the reaction atmosphere of 20% of O_2 in N_2 was not enough to improve the activity of the catalyst. The maximum selectivity to acrylic acid was of 15.8 %. The low yield of this product and the high selectivity to CO_x was related to the major formation of the unproductive $Mo_4V_6O_{25}$ crystalline phase.

In terms of CO_x selectivity, sample B, which was the first to show the presence of MoV_2O_8 (and is abundant in V_2O_5), showed the highest formation of CO_x due to the potential for formation of gas products (such as CO and CO_2). Indeed, the high concentration of vanadium in samples of mixed oxides is known to perform com-

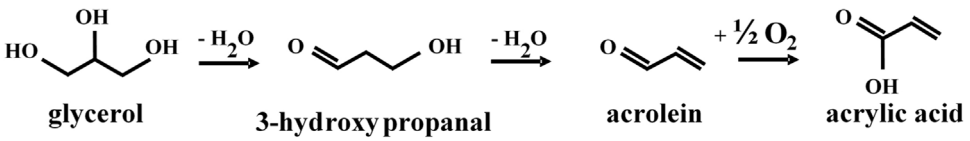

Scheme 2. Glycerol oxydehydration to acrylic acid on bifunctional acid-redox active sites.

Table 4
Catalytic activity of catalyst D in glycerol oxydehydration performed at 300 and 350 °C under a flow of 20% of O_2 in N_2.

		Catalyst D			
	Reaction temperature (°C)	300	350	300	350
	Precursors treated in a flow of	20% O_2/N_2	20% O_2/N_2	N_2	N_2
	Conversion (%)	71.8	96.9	67.3	87.3
Selectivity of products (%)	Acrolein	11.3	15.0	8.8	11.2
	Acrylic acid	15.6	32.0	4.0	15.8
	Acetic acid	2.6	16.3	4.2	5.8
	Acetaldehyde	2.6	10.9	3.0	6.8
	Minor by-products[a]	8.4	6.0	5.3	11.6
	CO and CO_2	59.5	19.8	74.7	48.8

[a] Minor products comprise the sum of products with selectivity lower than 2% such as acetol, propanal, allyl alcohol, 3-hydroxipropanal and propionic acid.

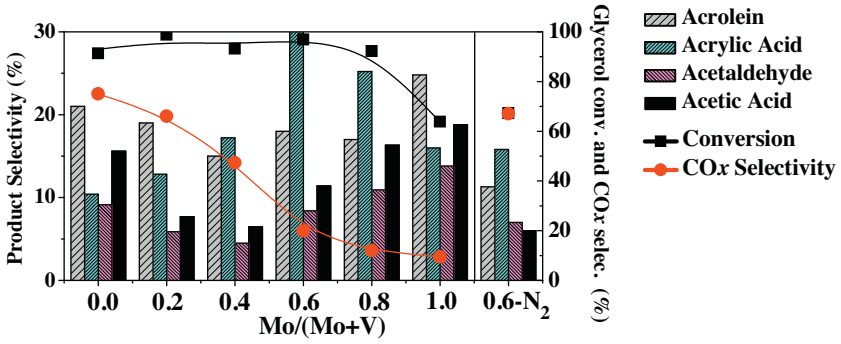

Fig. 8. Glycerol oxydehydration performed at 350 °C for 1 h and using 20% of O_2 in N_2 flow on mixed Mo-V oxides: Samples calcined in oxidizing (20% of O_2 in N_2, from A – 0.0 Mo/(Mo + V) – to F – 1.0 Mo/(Mo + V)) and inert atmosphere (100% of N_2, sample D-N_2 - 0.6 Mo/(Mo + V)).

plete oxidation, as disclosed in the publication of Patience et al. [50] As molybdenum was added to the catalyst, the CO_x selectivity approached 10%, from which it could be concluded that despite the oxidation potential of MoV_2O_8 and its appropriate redox cycle in the glycerol conversion to acrylic acid, MoV_2O_8 was not sufficiently oxidizing for the production of gas compounds.

Shen et al. [28] described similar results for glycerol oxydehydration with mixed oxides of vanadium and molybdenum, but found that the $Mo_6V_9O_{40}$ crystallographic phase (PDF 34-0527) was the most active. Another crystallographic phase was obtained due to the different conditions employed in the thermal treatment of the precursors. The findings of both studies reinforce the need to control the temperature and atmosphere during the treatments, because the final $Mo_xV_yO_z$ species, and consequently the active sites, are highly dependent on these conditions.

3.4. Stability test, optimization conditions, and spent catalyst analysis

Glycerol oxydehydration conducted over a period of 8 h and under a flow of 20% of O_2 in N_2 (Fig. 9a) indicated that the Sample D was not stable and deactivates due to aging. The deposition of polymerized glycerol byproducts (coking) was rejected after visual examination of the catalyst color and elemental CHN analysis indicate negligible amounts of carbon in the samples. Furthermore, an attempt to use carbon NMR revealed no carbon signal. The explanation for this deactivation behavior was associated with the crystallographic transformation of the most active phase MoV_2O_8 into $Mo_4V_6O_{25}$, as can be seen in the XRD pattern of Fig. 10. The MoV_2O_8 structure decreased from 61.0% to 7.5%, while the $Mo_4V_6O_{25}$ increased to 62.9%. The liquid products and CO_x selectivity also changed.

An attempt to maintain the oxidized MoV_2O_8 phase occurred by increasing the oxygen concentration in the reactor feed during glycerol oxydehydration (Fig. 9b). The concentration was increased from 20% to 100%. The catalyst showed steady activity and selectivity to acrylic acid, despite the increase in the selectivity to CO_x. The quantitative crystallographic phase analysis showed 36.1% of MoV_2O_8 and 33.8% of $Mo_4V_6O_{25}$ (*i.e.* ≅ 50% of each phase).

It seems that the balance of approximately 50/50% of $MoV_2O_8/Mo_4V_6O_{25}$ is achieved in the maximum performance of the catalyst obtained in these conditions. Moreover, as stated by other authors, the reduced state of vanadium in $Mo_4V_6O_{25}$ seems to improve the stability between the catalytic site and the intermediate acrylate ion adsorbed on the surface [40,51–53]. If no V^{4+} is present, acrylate adsorption is impaired, hence promoting total oxidation to CO_2 [49-51]. As a result, there is a relationship between increased selectivity towards acrylic acid and a low selectivity to CO_x. The differences between samples in selectivity are due to the altered redox features of the catalysts. Therefore, there is a compromise between reduced and oxidized phases, as pointed out by Figs. 9 a and 10 a and b.

In the first part of the study, the structural characterization of the temporal evolution of the mixed oxides of Mo-V was done for

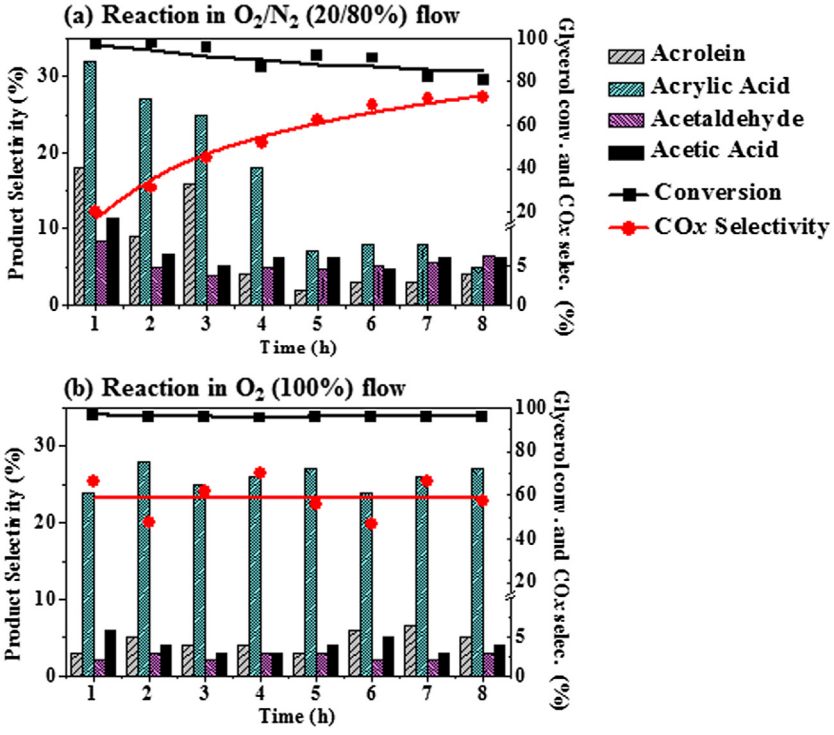

Fig. 9. Glycerol oxydehydration performed at 350 °C using Sample D calcined in oxidizing (20% of O_2 in N_2) atmosphere: (a) under a flow of 20% of O_2 in N_2 and (b) of pure O_2.

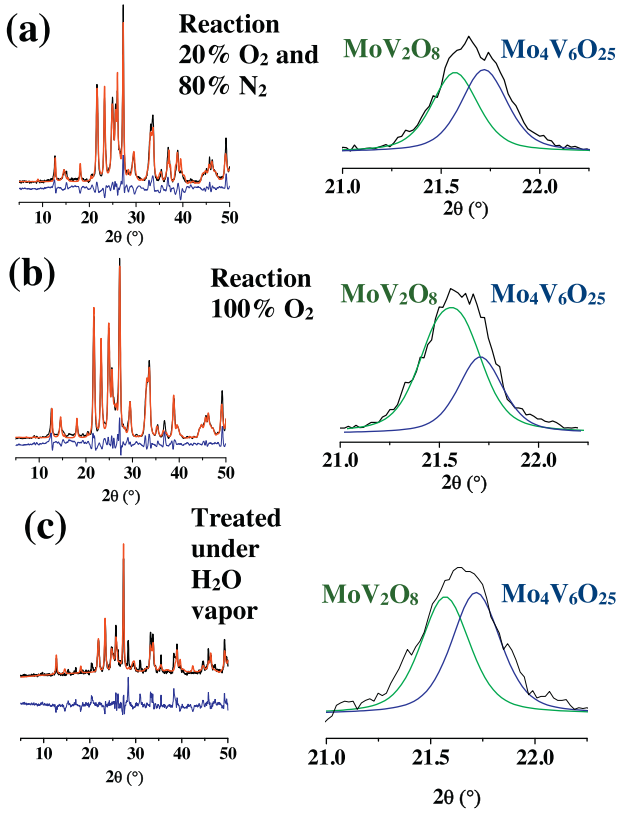

Crystalline Phase	Amount (%)
V_2O_5	5.0
MoO_3	24.6
$Mo_4V_6O_{25}$	62.9
MoV_2O_8	**7.5**

Crystalline Phase	Amount (%)
V_2O_5	2.0
MoO_3	28.1
$Mo_4V_6O_{25}$	33.8
MoV_2O_8	**36.1**

Crystalline Phase	Amount (%)
V_2O_5	0.0
MoO_3	53.5
$Mo_4V_6O_{25}$	25.3
MoV_2O_8	**21.1**

Fig. 10. X-ray diffractograms of spent sample D obtained after experiments of Fig. 9: (**a**) glycerol dehydration under a flow of 20% of O_2 in N_2, (**b**) under a flow of pure O_2, and (**c**) treated solely under water vapor. The green line represents the oxidized MoV_2O_8 phase, while the reduced $Mo_4V_6O_{25}$ are represented by the blue one. The results of quantitative phase analysis of each sample is also shown. (For interpretation of the references to colour in this figure legend, the reader is referred to the web version of this article.)

Table 5
Comparison of the oxydehydration catalysts, optimal conditions for glycerol conversion with maximum selectivity towards acrolein, acrylic acid and CO_x.

Catalyst	T (°C)	X glycerol (%)	Acrolein selectivity (%)	Acrylic acid selectivity (%)	CO_x selectivity (%)	Ref.
MoO_3	350	100	5	0	31	[28]
V_2O_5	350	100	12	5	67	[28]
V-W-Nb-O	296	100	2	11	76	[29]
V-Mo-O	300	90	10	20	38	[28]
V-W-O	300	100	0	24	55	[16]
V-W-O	310	100	11	25	39	[21]
V-W-O	300	90	20	26	31	[28]
V-Mo-O	300	100	3	26	35	[16]
V-Mo-Te-Nb-O	300	99	2	28	35	[16]
V-Mo-O (Sample D[a])	350	94	15	32	20	This work
$Mo_3VO_x/H_4SiW_{12}O_{40}/Al_2O_3$	300	100	3	46	33	[8]
V-W-Nb-O	265	100	3	50	32	[30]

[a] 1 h on stream of 20% of O_2 in N_2.

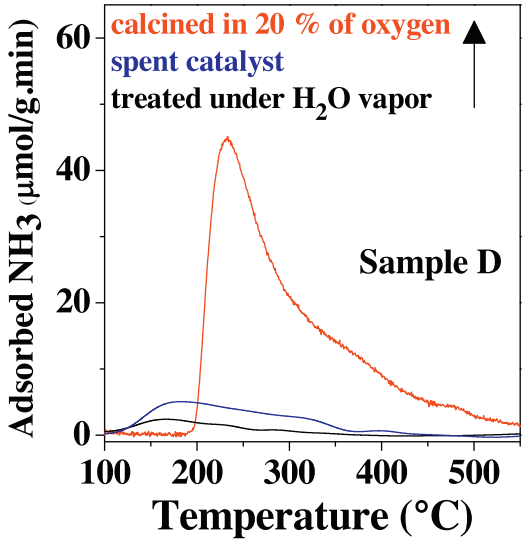

Fig. 11. TPD-NH_3 profiles of as-synthesized Sample D (calcined under a flow of 20 % of O_2 in N_2), spent sample D and water vapor treated sample D.

samples that have not been exposed to water vapor. In the second one, the catalytic experiments were conducted under a stream of 10 wt.% of glycerol in water. Even if no water should be used in the inlet stream, two water molecules are formed for each molecule of glycerol converted in the desired reaction and a higher stoichiometry of water to glycerol should be formed in unselective CO_x formation pathways. The consequence of water vapor in the catalytic performance of mixed oxides based on vanadium oxide is evident from the work of Ozaki et al.[54,55] that adsorbed hydroxyl groups play a role in partial oxidation catalysis. In the work of Wachs et al. [56] they showed that the presence of water has a pronounced effect on the molecular structures of the surface vanadium oxide species. In order to settle these remarks done by other authors we did measurements of ammonia desorption of Sample D in three different situations (Fig. 11). We compared samples (1) calcined in O_2/N_2 atmosphere, (2) after the catalytic oxydehydration of glycerol under O_2/N_2 atmosphere and (3) under a flow of water of 3 mL/h vaporized in the reactor entrance, in an attempt to simulate the reactions conditions under plenty of water. Although the sample history was different, it is clear that water vapor has considerable effect to promote changes on the structure of the mixed oxide from MoV_2O_8 to $Mo_4V_6O_{25}$, decreasing considerably not only the redox potential of the catalysts but also the quantity of acid sites. According to Ozaki *et al.* [55], the water molecule can dissociate on the surface of the catalyst making oxygen available for the catalytic reaction. This phenomenon leads to the reduction of V^{5+} sites and thereby decreasing the acidity of the catalyst. In fact, the diffractogram pattern in Fig. 10c confirms the effect of the water on the changes of the crystallographic phases (Fig. 10). However, an appropriate balance of $MoV_2O_8/Mo_4V_6O_{25}$ active phases can be preserved by feeding pure O_2 stream in the catalytic reactor.

Unfortunately, the addition of 100% of O_2 to regulate the active phases of mixed oxides of Mo and V led to an uncontrollable formation of CO_x up to 60%. The decomposition of glycerol and of the formed products is inevitable as reported in several studies (Table 5). Acrylic acid is the most abundant product, as depicted in Table 4 (32 % selectivity to acrylic acid in comparison to 15% of acrolein and 20% of CO_x), however the catalyst deactivates due to the change in the active phases of V-Mo-O. By feeding pure O_2 the active phases are preserved.

Finally, a fewpoints regarding other active phases are worth of consideration:

(1) Due to the fact that an amorphous phase is formed during the thermal treatment of the precursors of the catalysts at around 100 °C, it is quite possible that the samples have some quantities of amorphous phases of oxides of molybdenum and vanadium at the different heating stages of the experiments. These amorphous phases could have catalytic activity.
(2) Additionally, it was detected crystalline V_2O_5 and MoO_3, which could have interfacial surface with MoV_2O_8, and therefore a singular catalytic activity. In fact, an in depth analysis of Fig. 6 and 8 shows that the catalysts B (0.2 of Mo) and E (0.8 of Mo) contain the same amount of MoV_2O_8 (Fig. 6), but exhibit very different selectivity at the same conversion (Fig. 8). Sample E contains less V_2O_5 and more MoO_3 and is more selective. Similarly, this is true for the samples C and D.
(3) The synthesis of phase-pure samples of the phases was tried in order to correlate the catalytic performance individually, but it is almost impossible to do that. V_2O_5 and MoO_3 are the products of decomposition of the mixed oxides.

Concerning other redox systems, it has been shown in the literature that catalysts composed of the same single-phase may show different catalytic properties, because of different particle morphology for instance. Moreover, it has been demonstrated that the surface of crystalline oxidation catalysts under operation differs with respect to chemical composition and oxidation state from the bulk. However, in this current study, the combination of crystallographic quantification of phases of $Mo_yV_zO_x$ and catalytic performance in glycerol conversion pointed out that the crystalline phases of the mixed oxides are the main active phases. Noticeably, the catalytic performance changes at the same time in which the relative ratio between the crystalline phases $Mo_4V_6O_{25}$ and MoV_2O_8 changes. Therefore, the amorphous phases or the interfacial oxides seem to be very less active in the glycerol conversion to acrylic acid.

4. Conclusions

The thermal treatment of a mixture of ammonium paramolybdate and ammonium metavanadate resulted in the major formation of $Mo_xV_yO_z$ mixed oxides and minor quantities of V_2O_5, MoO_3, and MoO_2. The intermediate crystallographic phases were determined by *in situ* synchrotron X-ray diffraction under flows of 20% of O_2 in He or He alone. Up to 300 °C, the crystallographic speciation revealed identical transitional events that resulted in the key $NH_4Mo_4VO_{15}$ phase, from which the subsequent phases were formed. Above 300 °C, the increase of temperature caused an increase in N_2 production because of reduction reactions of the metals promoted by the NH_3 released from the precursors. The most reduced $Mo_4V_6O_{25}$ phase was formed under an inert atmosphere. On the other hand, the use of an oxygen atmosphere resulted in the oxidized vanadium and molybdenum atoms in MoV_2O_8.

In the glycerol oxydehydration to acrylic acid, the MoV_2O_8 phase was the most active, due to the driving force of the redox mechanism and the formation of oxygen vacancies in this compound. The greater activity of MoV_2O_8 could be explained by the formation of vacancies around vanadium atoms (changes in the oxidation state of vanadium), because changes in molybdenum valence remained stable, as shown by the XAS and XPS analyses.

During the catalytic conversion of glycerol into acrylic acid the catalyst deactivates due to the crystallographic transformation of the most active phase MoV_2O_8 into $Mo_4V_6O_{25}$. This is caused by the presence of water vapor that dissociates on the surface of the catalyst and leads to the reduction of V^{5+} sites. However, an appropriate balance of $MoV_2O_8/Mo_4V_6O_{25}$ active phases can be maintained by feeding pure O_2 stream in the catalytic reactor, allowing a long-time stability of the catalysts for the selective conversion of glycerol.

Acknowledgements

This work was supported by the Brazilian agencies CNPq (grants 473346/2012-5 and 401679/2013-6) and FAPESP (grants 2010/01449-3, 2013/10204-2 and 2013/50023-7). The authors also thank the Brazilian Synchrotron Light Laboratory (LNLS) in Campinas for use of the XAFS1 and XPD beamlines (proposals XAFS1-16110 and XPD-17839), and Dr Peter Hammer of LEFE/UNESP for performing the XPS analyses.

Appendix A. Supplementary data

Supplementary data associated with this article can be found, in the online version, at http://dx.doi.org/10.1016/j.apcata.2016.12.010.

References

[1] X. Xu, J. Lin, P. Cen, Chin. J. Chem. Eng. 14 (2006) 419–427.
[2] B. Katryniok, S. Paul, F. Dumeignil, ACS Catal. 3 (2013) 1819–1834.
[3] L.G. Possato, R.N. Diniz, T. Garetto, S.H. Pulcinelli, C.V. Santilli, L. Martins, J. Catal 300 (2013) 102–112.
[4] M.V. Rodrigues, C. Vignatti, T. Garetto, S.H. Pulcinelli, C.V. Santilli, L. Martins, Appl. Catal., A: G: Gen. 495 (2015) 84–91.
[5] J. Cecilia, C. García-Sancho, J. Mérida-Robles, J. Santamaría-González, R. Moreno-Tost, P. Maireles-Torres, Catal. Today 254 (2015) 43–52.
[6] H. Decolatti, B. Dalla Costa, C. Querini, Microporous Mesoporous Mater. 204 (2015) 180–189.
[7] X. Feng, Y. Yao, Q. Su, L. Zhao, W. Jiang, W. Ji, C.-T. Au, Appl. Catal. B-Environ. 164 (2015) 31–39.
[8] L. Liu, B. Wang, Y. Du, A. Borgna, Appl. Catal. A: Gen. 489 (2015) 32–41.
[9] S.-H. Chai, H.-P. Wang, Y. Liang, B.-Q. Xu, Green Chem. 9 (2007) 1130–1136.
[10] H. Atia, U. Armbruster, A. Martin, J. Catal. 258 (2008) 71–82.
[11] W. Suprun, M. Lutecki, T. Haber, H. Papp, J. Mol. Catal. A: Chem. 309 (2009) 71–78.
[12] F. Wang, J.-L. Dubois, W. Ueda, J. Catal. 268 (2009) 260–267.
[13] L.H. Vieira, K.T. Carvalho, E.A. Urquieta-González, S.H. Pulcinelli, C.V. Santilli, L. Martins, J. Mol. Catal. A: Chem. 422 (2015) 148–157.
[14] L.G. Possato, W.H. Cassinelli, T. Garetto, S.H. Pulcinelli, C.V. Santilli, L. Martins, Appl. Catal. A: Gen. 492 (2015) 243–251.
[15] C.F.M. Pestana, A.C.O. Guerra, G.B. Ferreira, C.C. Turci, C.J.A. Mota, J. Braz. Chem. Soc. 24 (2013) 100–105.
[16] J. Deleplanque, J.L. Dubois, J.F. Devaux, W. Ueda, Catal. Today 157 (2010) 351–358.
[17] W. Ueda, J. Jpn. (2013) 122–132.
[18] S. Ishikawa, X.D. Yi, T. Murayama, W. Ueda, Catal. Today 238 (2014) 35–40.
[19] K. Omata, K. Matsumoto, T. Murayama, W. Ueda, Chem. Lett. 43 (2014) 435–437.
[20] C.T. Qiu, C. Chen, S. Ishikawa, T. Murayama, W. Ueda, Top. Catal. 57 (2014) 1163–1170.
[21] M. Dolores Soriano, P. Concepcion, J.M. Lopez-Nieto, F. Cavani, S. Guidetti, C. Trevisanut, Green Chem. 13 (2011) 2954–2962.
[22] A.S.P. Paula, L.G. Possato, D.R. Ratero, K. Keinan-Adamsky, R.R. Soares, G. Goobes, L. Martins, J.G. Nery, Microporous Mesoporous Mat. 232 (2016) 151–160.
[23] K. Omata, K. Matsumoto, T. Murayama, W. Ueda, Catal. Today 59 (2016) 205–212.
[24] L.G. Possato, T.F. Chaves, W.H. Cassinelli, S.H. Pulcinelli, C. Santilli, L. Martins, Catal. Today (2016), http://dx.doi.org/10.1016/j.cattod.2016.08.005.
[25] B. Katryniok, S. Paul, M. Capron, C. Lancelot, V. Belliere-Baca, P. Rey, F. Dumeignil, Green Chem. 12 (2010) 1922–1925.
[26] B. Katryniok, S. Paul, V. Belliere-Baca, P. Rey, F. Dumeignil, Green Chem. 12 (2010) 2079–2098.
[27] P. Mars, D.W. Van Krevelen, Chem. Eng. Sci. 3 (1954) 41–59.
[28] L. Shen, H. Yin, A. Wang, X. Lu, C. Zhang, Chem. Eng. J. 244 (2014) 168–177.
[29] A. Chieregato, F. Basile, P. Concepcion, S. Guidetti, G. Liosi, M. Dolores Soriano, C. Trevisanut, F. Cavani, J.M. Lopez-Nieto, Catal. Today 197 (2012) 58–65.
[30] A. Chieregato, M. Dolores Soriano, F. Basile, G. Liosi, S. Zamora, P. Concepcion, F. Cavani, J.M. Lopez-Nieto, Appl. Catal. B-Environ. 150 (2014) 37–46.
[31] A. Chieregato, M.D. Soriano, E. Garcia-Gonzalez, G. Puglia, F. Basile, P. Concepcion, C. Bandinelli, J.M.L. Nieto, F. Cavani, Chemsuschem 8 (2015) 398–406.
[32] T.V. Andrushkevich, T.G. Kuznetsova, Kinet. Catal. 27 (1986) 571–578.
[33] J. Tichy, Appl. Catal. A: Gen. 157 (1997) 363–385.
[34] H. Canova, A. Fontoura, R. Neuenschwander, B. Diaz, C. Rodella, J. Phys. Conf. Ser. IOP Publishing (2014) 012004.
[35] B. Toby, J. Appl. Crystallogr. 34 (2001) 210–213.
[36] A.F. Gualtieri, S. Ferrari, M. Leoni, G. Grathoff, R. Hugo, M. Shatnawi, G. Paglia, S. Billinge, J. Appl. Crystallogr. 41 (2008) 402–415.
[37] G. Leofanti, M. Padovan, G. Tozzola, B. Venturelli, Catal. Today 41 (1998) 207–219.
[38] T. Ressler, O. Timpe, T. Neisius, J. Find, G. Mestl, M. Dieterle, R. Schlogl, J. Catal. 191 (2000) 75–85.
[39] E.M. Thorsteinson, T.P. Wilson, F.G. Young, P.H. Kasai, J. Catal. 52 (1978) 116–132.
[40] T.P. Gorshkova, D.V. Tarasova, I.P. Olenkova, T.V. Andrushkevich, T.A. Nikoro, Kin. Catal. 25 (1984) 158–162.
[41] M. Sadakane, K. Kodato, T. Kuranishi, Y. Nodasaka, K. Sugawara, N. Sakaguchi, T. Nagai, Y. Matsui, W. Ueda, Angew. Chem. Int. Ed. 47 (2008) 2493–2496.
[42] V.A. Zazhigalov, S.V. Khalameida, N.S. Litvin, I.V. Bacherikova, J. Stoch, L. Depero, Kin. Catal. 49 (2008) 692–701.
[43] G. Dabrowska, P. Tabero, M. Kurzawa, J. Phase Equilib. Diffus. 30 (2009) 220–229.
[44] E.J. Whittake, R. Muntus, Geochim. Cosmochim. Acta 34 (1970) 945–956.
[45] K.T. Li, M.Y. Huang, W.D. Cheng, Ind. Eng. Chem. Res. 35 (1996) 621–626.
[46] T.M. Sankaranarayanan, R.H. Ingle, T.B. Gaikwad, S.K. Lokhande, T. Raja, R.N. Devi, V. Ramaswamy, P. Manikandan, Catal. Lett. 121 (2008) 39–51.
[47] G. Terán-Escobar, J. Pampel, J.M. Caicedo, M. Lira-Cantú, Energy Environ. Sci. 6 (2013) 3088–3098.
[48] V. Bondarenka, S. Kaciulis, Z. Martunas, A. Reza, G.J. Babonas, A. Pasiskevicius, Lith. J. Phy. 48 (2008) 341–348.
[49] Y.S. Yun, K.R. Lee, H. Park, T.Y. Kim, D. Yun, J.W. Han, J. Yi, ACS Catal. (2014).
[50] G.S. Patience, R.E. Bockrath, J.D. Sullivan, H.S. Horowitz, I&EC Resear, (2007) 4374–4381.
[51] T.V. Andrushkevich, L.M. Plyasova, G.G. Kuznetsova, V.M. Bondareva, T.P. Gorshkova, I.P. Olenkova, N.I. Lebedeva, React. Kinet. Catal. Lett. 12 (1979) 463–467.
[52] T.G. Kuznetsova, G.K. Boreskov, T.V. Andrushkevich, L.M. Plyasova, N.G. Maksimov, I.P. Olenkova, React. Kinet. Catal. Lett. 12 (1979) 531–536.
[53] T.G. Kuznetsova, G.K. Boreskov, T.V. Andrushkevich, Y.A. Grigorkina, N.G. Maksimov, I.P. Olenkova, L.M. Plyasova, T.P. Gorshkova, React. Kinet. Catal. Lett. 19 (1982) 405–409.
[54] Y. Moro-Oka, Y. Takita, A. Ozaki, J. Catal. 27 (1972) 177–184.
[55] T.Y. Takita, Y. Moro-Oka, A. Ozaki,;1 J. Catal. 52 (1978) 95–101.
[56] J.M. Jehng, G. Deo, B.M. Weckhuysen, I.E. Wachs, J. Mol. Catal. A: Chem. 110 (1996) 41–54.